



Bentonite-free water-based drilling fluids at HP/HT condition: a rheometric analysis

Luis H. Quitian¹ · Diogo E. V. Andrade² · Admilson T. Franco¹

Received: 10 March 2022 / Revised: 8 June 2022 / Accepted: 9 June 2022 / Published online: 27 June 2022
© The Author(s), under exclusive licence to Springer-Verlag GmbH Germany, part of Springer Nature 2022

Abstract

The bentonite-free water-based drilling fluid aids in reducing formation damage in offshore operations in ultra-deep wells. In this scenario, the material experiences high-pressure and high-temperature conditions. The material's rheological behavior may be affected not only by the temperature but also by the pressure. Knowing the influence of these variables on the drilling fluid's rheological characteristics is essential for successfully planning and executing the drilling process. This paper investigates the effect of pressure, temperature, and thermal aging in the liquid-like and solid-like regimes of a bentonite-free water-based drilling fluid. The main viscosifier in the fluid is xanthan gum. The experiments were carried out in a pressure cell coupled to a rotational rheometer. The results show a more relevant impact of temperature than pressure on the rheological behavior of the drilling fluid. The experiments also exhibit a critical aging temperature that induces irreversible fluid degradation. Lastly, these findings bring relevant information over an efficient range of bentonite-free water-based drilling fluids employed in the offshore drilling process.

Keywords Bentonite-free water-based drilling fluid · Xanthan gum · High-pressure · High-temperature · Aging temperature

Introduction

The oil and gas exploration industry faces extreme conditions in high-pressure and high-temperature (HP/HT) wells (Bottom-hole temperature over 150 °C and pressure over 700 bar) (Greenaway et al. 2008). The drilling process requires knowledge of the drilling fluid's rheological

behavior under these conditions. One crucial role of these fluids is to transport the cutting out of the well and keep the cutting suspended in the fluid during the process stoppages (Njobuenwu and Wobo 2007; Fernandes et al. 2017a). To fulfill these requirements, the drilling fluids are formulated to present a solid-like behavior below the yield stress and a liquid-like behavior above this point. In the solid-like regime, the material's deformation is limited under stress, while it flows like a liquid for shear stresses higher than the critical one. Due to its formulation, drilling fluids are elastoviscoplastic materials, exhibiting yield stress, shear-thinning behavior, and thixotropy (Mewis and Wagner 2012; Andrade et al. 2016; Fernandes et al. 2016).

Historically, water-based drilling fluids (WBDF) were first used in well drilling operations. The high energy demand leads to synthetic oil-based drilling fluids being the most used. Due to economic reasons and environmental regulations, the petroleum industry has increased its interest in WBDF, mainly in drilling wells involving HPHT (Seymour and Macandrew 1994). WBDF with clays (bentonite, laponite, etc.) as a viscosifier presents good thermal stability and lubrication (Njobuenwu and Wobo 2007; Raheem and Vipulanandan 2019). However, this drilling fluid has some issues related to fluid losses and damage to the reservoir. The

✉ Admilson T. Franco
admilson@utfpr.edu.br

Luis H. Quitian
luis.2019@alunos.utfpr.edu.br

Diogo E. V. Andrade
diogo.andrade@ufrgs.br

¹ Academic Department of Mechanics – DAMEC, Postgraduate Program in Mechanical and Materials Engineering – PPGEM, Research Center for Rheology and Non-Newtonian Fluids – CERNN, Federal University of Technology – Paraná – UTFPR, R. Deputado Heitor Alencar Furtado, 5000 - Bloco N - Ecoville, Curitiba, PR 81280-340, Brazil

² Department of Mechanical Engineering – DEMEC, Rheology and Non-Newtonian Fluid Flow Laboratory – ReoSul, Federal University of Rio Grande Do Sul - UFRGS, Rua Sarmento Leite 425, Porto Alegre, RS 90050-170, Brazil

invasion of deformable solid particles that cause swelling/dispersion of the clay particles in the reservoir could lead to serious adverse effects. The high clay content in HPHT conditions causes excess torque and drag, reducing the rate of penetration and significantly increasing formation damage (Song et al. 2016). In other words, the migration of clay through the formation can accumulate in the pore throats reducing the reservoir permeability. This damage can be irreversible and may have a severe economic impact on reservoir productivity (Bagci et al. 2000; Wilson et al. 2014).

The clay-free water-based drilling fluid (CF-WBDF) formulations are designed as candidates to replace bentonite-based and laponite-based drilling fluids. These formulations employ polymers to achieve satisfactory performance during the drilling operation and keep the clay-based drilling fluids' main rheological characteristics and filtration properties (Huang et al. 2016). CF-WB drilling fluids composed of synthetic polymers such as polyacrylamides, N-vinylcaprolactam, and related derivatives are used for operations in HPHT conditions to replace the clay option (Xie et al. 2016). These additives are used to increase the fluid's resistance at high temperatures, but the downside is the high costs involved in these formulations. Another usual low-cost alternative is biopolymers such as xanthan gum (XG). The additive XG is used to aid in achieving the desired drilling fluid rheological properties and also has the function of minimizing formation damage (Navarrete et al. 2000; Zhou et al. 2015; Xia et al. 2020).

The implementation of XG solutions in drilling fluid showed that it always provides high-viscosity, yield stress, shear-thinning behavior, and high resistance to shear degradation, improving the properties of the drilling fluid and reducing formation damage (Fitzpatrick et al. 2013; Wei et al. 2014; Jang et al. 2015; Sofia and Djamel 2016; N'gouamba et al. 2021). Its rheological properties depend on the concentration of the biopolymer (N'gouamba et al. 2021), the salt concentration (Wu et al. 2021), and the temperature (Zhong et al. 2006). A recent study (N'gouamba et al. 2021) showed that these materials could present a rheopectic behavior at high concentrations, i.e., its viscosity increased with time for given shear stress. The main restriction of using xanthan gum in drilling fluids is the possibility of thermal degradation. This material presents a natural conformation with an order-to-disorder transition at high temperatures, called conformational transition temperature (T_m) (Wu et al. 2021). Many advances have been obtained in the sense of increasing the transition temperature by adding some additives to the drilling fluid and ultimately extending the range of temperature in which the XG-based drilling fluid can be used (Wu et al. 2021; Zhu and Zheng 2021).

Some research currently proposes increasing XG's thermal resistances using formate brine (sodium, potassium, and cesium salts of formic acid), especially for fluids without a

clay base (Sukhoboka 2017; Leusheva and Alikhanov 2021). Salts such as potassium formate are non-toxic and environmentally friendly salts that do not cause formation damage. This type of salt used in high-temperature applications provides structural stability to biopolymers and greater thermostability to drilling fluids (Sukhoboka 2017; Leusheva and Alikhanov 2021; Morenov et al. 2021). On the other hand, some results showed that brine formate causes flocculation of clay minerals in the well, causing a high volume of filtrate and high thixotropy (Quainoo et al. 2020).

Other studies such as the one by Zhu and Zheng (2021) mention that high concentrations of NaCl, which is the predominant salt on the rocky surface, affect the conformational transition temperature and the double helix structure of XG which further affects the rheological and filtration properties, increasing viscosity and reducing filtration volume (Wu et al. 2021). Although many researchers have discussed the influence of high temperature in the water-based drilling fluid (WBDF) in which the xanthan gum is used as an additive (Seright and Henrici 1986; Howard et al. 2015; Reinoso et al. 2019; Wu et al. 2021; Zhu and Zheng 2021), one cannot find a study on the influence of pressure and temperature on bentonite-free water-based drilling fluids (BF-WBDF) with xanthan gum.

The current study aims to analyze the rheological behavior of BF-WBDF with xanthan gum as an additive and NaCl brine which can be found in large quantities in offshore drilling in HPHT regions. As far as we know, the use of BF-WBDF with XG as the main viscosifier has been studied by Vargas et al. (2020) with a mixture of nanoparticles; but a rheological analysis at high temperatures and pressures has not yet been conducted in the literature. To fill this gap, we analyzed and discussed the effect of high pressures and high temperatures on the rheological characteristics of a BF-WBDF in the liquid-like and solid-like regimes. This paper starts by describing the equipment and methodology used in the analyses, then the influence of the pressure and temperature are presented, followed by the main conclusions.

Materials and methods

The samples used in the current work consisted of bentonite-free water-based drilling fluid with a density of 1160 kg/m³, kindly provided by Petrobras. The fluid is composed of xanthan gum, NaCl brine, high-performant starch, and other components presented in Table 1, the specific composition is not mentioned due to supplier confidentiality. Before each experiment, the drilling fluid was homogenized for 20 min at 1000 rpm with a low-capacity industrial mixer (Hamilton Beach HMD200).

The rheometrical tests were performed on a rotational stress-controlled rheometer Anton Paar MCR 502 (Anton

Table 1 Composition of bentonite-free water-based drilling fluid with xanthan gum

Composition	Concentrations	Unit
Industrial water—QSP	QSP*	-
NaCl brine	156.7	kg/m ³
Anti-foamer (Polifoan)	1.19	ml/m ³
Xanthan Gum	5.7	kg/m ³
Starch HP	22.8	kg/m ³
Magnesium oxide	4.3	kg/m ³
Lubricant (Liovac 4260)	2	% v/v
Bactericidal (Polibac TC)	1.4	kg/m ³
Magnesium peroxide	2.8	kg/m ³
Rheological Modifier (BDF 990)	2.8	kg/m ³
Limestone Ca(OH) ₂	QSP* p/1.51	m ³

QPS*, qualified stormwater pollution prevention plan practitioner

Paar Co., Austria). The rheometer was used with two different configurations: (i) standard configuration and (ii) with a pressure cell coupled in the rheometer, as presented in Fig. 1.

As shown in Fig. 1, the pressurization system is composed of a pressure supply unit with a 400-bar hand pump (1) that transmits a pre-pressure to the cylinder of a spindle pump (2) responsible for increasing the pressure up to 1000 bar. Following, the pressure is transferred to the

drilling fluid through a unit separator (3) that induces the pressure up to the pressure head (4) and the pressure cup (5), which are coupled to the rheometer. The measurement cell used a magnetic coupling (6) that transfers the torque from the motor drive to the internal mounted inside in the pressure cup (5) with sapphire bearings at the extremities. The Couette geometry presents roughened surfaces, with an internal cylinder diameter of 28 mm, a height of 50 mm, and a cup diameter of 30 mm.

As the absence of a mechanical coupling reduces the sensitivity of the measurements at low torques and rotations, the experiment was first carried out in the standard configuration MCR 502 rheometer also using a Couette roughened surfaces geometry (internal cylinder diameter of 20 mm, the height of 30 mm, and diameter cup of 22 mm). These experiments were executed in triplicate to have a reference. Statistical significance was verified through analysis of variance (ANOVA with $\alpha=0.05$), where it was evidenced that the repetitions are statistically significant (p -value = 0.01675).

After that, the same experiments were executed in the pressure cell at atmospheric pressure. With both results in hand, we can determine the range of shear stress and shear rate in which the results obtained with the pressure cell configuration are reliable. Then, the experiments performed at high pressures are strictly analyzed in this reliable range.

Before each experiment, the sample was loaded inside the geometry. The whole system is closed. A pre-shear of

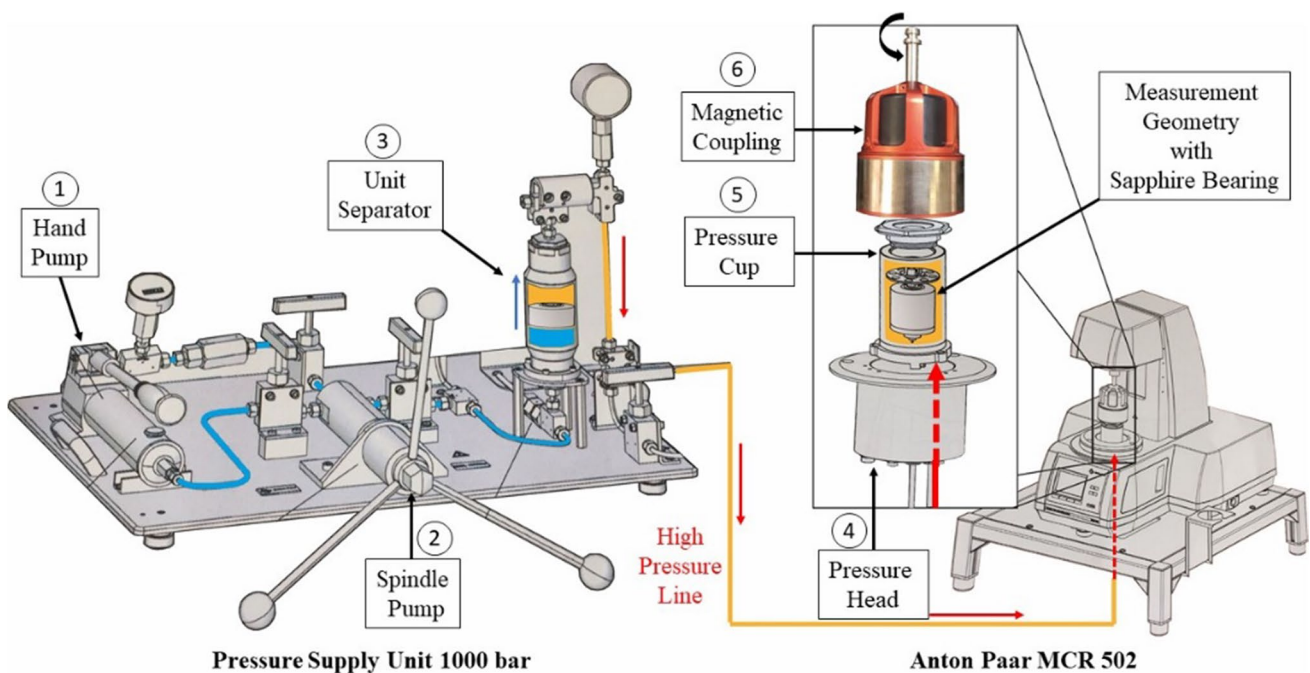


Fig. 1 Pressurization system used to increase pressures up to 1000 bar, connected to the Anton Paar MCR 502 rheometer, and pressure cell with magnetically coupled geometry with sapphire bearing.

Adapted from the Instruction Manual C-ETD 300/PR 1000 (Paar 2015). The drilling fluid is represented in yellow, and the pressurized oil is in blue

600 s⁻¹ for 10 min was applied to the sample, and the material was left at rest (zero shear stress) for 10 min. The resting time allows the material restructuration. The goal of the pre-test is to induce a known and similar shear history in all samples. In other words, the sample was at the same reference state before each test.

Thermal aging protocol

Thermal aging was conducted to analyze the aging process at high temperatures. The sample was carried out in the Roller Oven Fann stove, using an aging cell, pressurized to 6-bar to avoid boiling the sample. It is important to emphasize that water boils at around 160 °C at 6-bar (Fann Instrument Company 2014). A 400-ml sample is used for each test, previously homogenized and inserted into the aging cell. Then, tests were developed following the API 13B-1 (API Recommended Practice 13B-1 2017) standard procedure for dynamic aging tests for 16 h. Finally, the aged fluid is removed from the cell and left in a closed bottle for 24 h at room temperature. After that, the aged sample was tested in the rheometer.

Rheometric experiments

Flow curves

The first point to be analyzed is the material behavior at a steady state by determining the flow curve at different temperatures and pressures. These experiments were conducted by imposing a series of constant shear rate levels ranging from 0.1 to 400 s⁻¹ for 1000 s each of the shear rates, which is enough time for the material to reach the steady-state regime. The variations of the apparent viscosity as a function of time for each shear rate plateau are presented in Appendix 2. As in this specific experiment, we are focusing on the steady-state results; the plateaus of shear rates were distributed using a high shear rate between two low values to avoid sedimentation (i.e., 400, 0.1, 350, 1, 300, 5, 250, 10, 200, 50, 150, 100 s⁻¹). It is worth mentioning that this protocol was developed thanks to a series of experimental comparisons that were carried out in the laboratory. We can state that the sequence of the imposed shear rate does not affect the measured flow curve for this drilling fluid. Moreover, the high shear rate imposed between two low values prevented the sedimentation.

Oscillatory shear stress amplitude sweeps

Another essential point to be analyzed is how the pressure affects the material's behavior in the solid-like regime. The knowledge of the influence of pressure on the gel strength is essential for the start-up procedure after process stoppages.

In order to accomplish this objective, oscillatory experiments were performed. The material was pre-sheared and rested for 10 min. Then, stress amplitude oscillatory sweep tests (from 0.001 to 100 Pa) were carried out at 25 °C and 1 Hz. The experiments were conducted for the same pressure levels used in the viscosity flow curve.

Rheological models

The experimental data obtained were fitted to the power-law model. The model fits two parameters known as the consistency coefficient (m), which represents the viscosity modifications under different conditions, and the flow behavior index (n), which represents the structural characteristics of the fluid (Ansari et al. 2020; Patrick et al. 2021) [Eq. 1]. For the process of modeling the behavior of pressure and temperature, equations were used that describe the evolution of viscosity with these variables. The coefficients m and n were found using nonlinear regression of the average viscosity data weighted with the standard deviation. The methodology considers the variations in the experimental data as the regression error when evaluating the regression parameters. Thus, it was possible to generate the parameters m and n , in addition to the parameter's uncertainties (δm and δn) for fitting the viscosity in a confidence interval of 95%. Besides, ANOVA analysis is performed for each fit.

$$\eta(\dot{\gamma}) = m \cdot [\dot{\gamma}]^{n-1} \quad (1)$$

For pressure, the Barus equation was used, which relates the exponential variation of the viscosity-pressure coefficient “ α ” with the variation of pressure and empirical parameter “ A ” [Eq. 2]. This equation was modified by adding other empirical fit parameter “ B ” [Eq. 3] for a better fit.

$$\eta(P) = A \cdot \exp(\alpha P) \quad (2)$$

$$\eta(P) = B + A \cdot \exp(\alpha P) \quad (3)$$

For temperature, the WLF model was used for the evolution of viscosity [Eq. 4]. The model is an empirical equation associated with temperature superposition, relating the viscosity to the reference temperature “ η_0 ,” two empirical parameters (C_1 and C_2) and temperature variations with reference temperature “ T_0 .”

$$\eta(T) = \eta_0 \cdot 10^{\left(\frac{-C_1(T-T_0)}{C_2+T-T_0}\right)} \quad (4)$$

Results and discussion

We first present the influence of the pressure on the rheological behavior of the drilling fluid, then we investigate the effects of temperature imposed on the rheometer and, finally, the influence of the aging process at high temperatures.

Influence of the pressures

Firstly, the influence of the pressure on the material's apparent viscosity. Primarily we must determine the reliable range in which the pressure cell configuration can be used adequately. The experiments were performed using the pressure cell configuration (P.C) and the standard configuration (S.C) both at atmospheric pressure and 25 °C. Figure 2(a) shows the apparent viscosity as a function of the shear rate for both conditions.

As can be observed in Fig. 2(a), the bentonite-free water-based drilling fluid with xanthan gum shows a shear-thinning behavior as previously reported in the literature (Whitcomb and Macosko 1978; Sofia and Djamel 2016; Zheng et al. 2020), meaning that the higher the shear rate, the lower the apparent viscosity. One can also see that the pressure cell configuration results are pretty similar to the standard configurations ones in the range from 400 to 50 s⁻¹. For values

lower than 50 s⁻¹, the pressure cell could not measure the same results as the reference. From these values down, the measured torque must be too low for the sensibility of the magnetic coupling system. In all the pressure cell configuration analyses, the experiments were carried out in the reliable range determined by this comparison (from 400 to 50 s⁻¹).

After determining the lowest shear rate to be implemented in the pressure cell configuration, the effect of pressure is now analyzed through steady-state viscosity flow curves, as presented in Fig. 2(b). In all the investigated ranges of imposed pressure, the apparent viscosity showed a slight increment with increasing pressure. The apparent viscosity increment was roughly the same (i.e., around 1.4 times from atmospheric pressure to 800-bar).

The influence of the pressure on the apparent viscosity can also be evaluated by fitting the experimental data. The power-law equation and a modified Barus' model were used to fit the piezo-viscous effect (Chaudemanche et al. 2009; Hermoso et al. 2014). Figure 2(b) displays the results of the fitted equation (black-dashed lines), obtaining a mean square error of less than 4%. The power-law equation was fitted for each one of the imposed pressures. Table 2 shows the parameters of the power-law equation fitted with the respective correlation coefficient (*R*²). All fits are statistically significant since their *p*-value < 0.001, hence, the combined

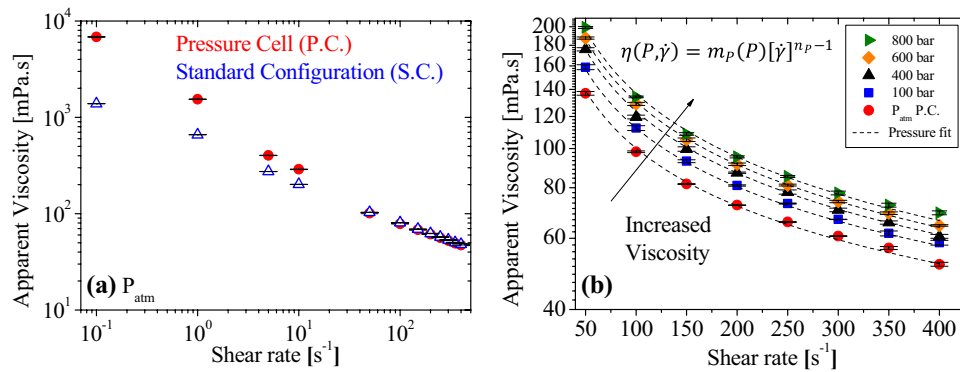


Fig. 2 Comparison of the (a) steady-state viscosity flow curve at 25 °C and atmospheric pressure obtained on the Anton Paar rheometer with the pressure cell (red circles) and standard configuration (blue hollow triangles), (b) steady-state viscosity curve at a different

pressure from atmospheric pressure to 800 bar at 25 °C along with the best fit of the modified power-law equation. The error bars denote the standard deviation of experiments performed in triplicate

Table 2 Fitted parameters of the power-law equation for different pressures. Consistency coefficient (*m_p*), flow behavior index (*n_p*), parameter uncertainties (*δm_p* and *δn_p*), Mean squared error (MSE), and correlation coefficient (*R*²)

Pressure	<i>m_p</i> [Pa.s ⁿ]	<i>δm_p</i> [Pa.s ⁿ]	<i>n_p</i> [-]	<i>δn_p</i> [-]	MSE	<i>R</i> ²
Atmospheric pressure	886.7	19.67	0.53	0.005	2.42	0.997
100 bar	1048.8	13.41	0.52	0.002	0.27	0.998
400 bar	1272.7	43.48	0.49	0.007	2.25	0.998
600 bar	1405.6	27.77	0.48	0.004	0.85	0.999
800 bar	1520.7	67.95	0.48	0.009	4.80	0.997

expanded uncertainty of the viscosity and pressure measurements at the 95% confidence level.

First, all the fits were adequately representative, with a correlation coefficient greater than 0.99. Afterward, it can be observed that as the pressure increases, the consistency coefficient increases, representing an increase in the apparent viscosity, as observed in Fig. 2(b). In contrast, the flow behavior index (n_p) is roughly independent of the pressure, i.e., $n_p \approx 0.5$. For obtaining a unique fitted equation for the range of pressures, the consistency coefficient (m) values determined in each pressure were fitted using a modified model based on the Barus equation, which depends on the variations of “ m_p ” with pressure (Fig. 3). This model presented a power behavior with a correlation coefficient of 0.994. This value of R^2 shows us that the predicted values of viscosity as a function of pressure were good, as shown in Appendix 3, which compares the predicted values by the model and the measured experimental values. Once that, the apparent viscosity changes can be represented by any pressure and shear rate. One needs to first determine the consistency coefficient for the desired pressure

[$m_p(P) = 1849.35 - 945.06 \exp(-0.0013P)$] and then use this value to determine the apparent viscosity at the desired shear rate [$\eta(P, \dot{\gamma}) = m_p(P) \dot{\gamma}^{0.5}$].

It is also noteworthy that the influence of the pressure on the apparent fluid viscosity is more impactful in the low magnitude range. Observing the fitted curve, the higher the pressure magnitude, the lower the impact on the consistency coefficient for the same pressure increment. As William et al. (2014) reported, the polymer molecules are compressed as the pressure increases.

In order to analyze the role of the pressure on the behavior of the material in the solid-like regime, oscillatory shear stress amplitude sweeps tests were performed. In these analyzes, dynamic moduli (G' and G'' —y-axis) were investigated as a function of stress amplitude (x-axis), as can be seen in Fig. 4(a) for both rheometer configurations.

In this experiment, the material behavior is allocated to the linear viscoelastic region at low values of imposed stress amplitude. In this region, called SAOS (Small Amplitude Oscillatory Shear), the storage modulus (G') is higher than the viscous modulus (G''), and both are independent of the imposed stress. The material’s mechanical response can also be analyzed by the phase angle shift [$\delta = \text{atan}(G''/G')$], which compares the magnitudes of G' and G'' . The material behaves as a purely viscous fluid if $\delta = 90^\circ$ and as an elastic solid if $\delta = 0^\circ$. For $0^\circ < \delta < 90^\circ$, it is a viscoelastic material (Macosko 1994). The result shows some nonlinearities at a certain stress level to the beginning of irreversible plastic deformations of the material (Fernandes et al. 2017b; Donley et al. 2020). This is the MAOS (Medium Amplitude Oscillatory Shear) in which G' and G'' depend on the imposed shear stress. Finally, the material reaches the LAOS regime (Large Amplitude Oscillatory Shear), and one can observe the $G'-G''$ crossover. Although, by definition, the dynamic moduli can only be checked in the SAOS regime, and the effect in the gel breaking of the shear history imposed in the MAOS and LAOS regime is complex to be thoroughly analyzed, some experimental evidence shows that the crossover stress can be used as a reasonable estimation of the material gel strength (Fernandes et al. 2017b).

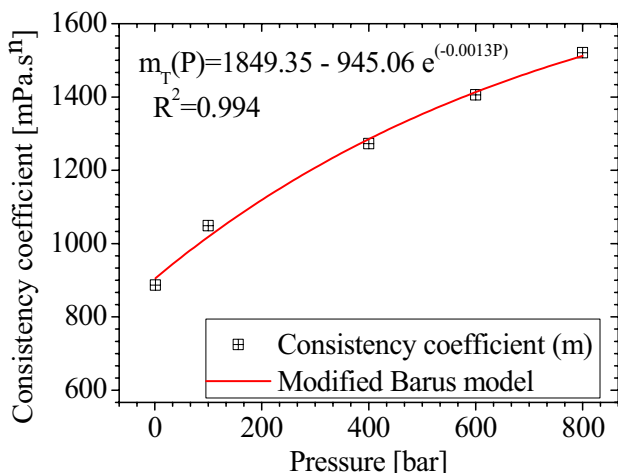
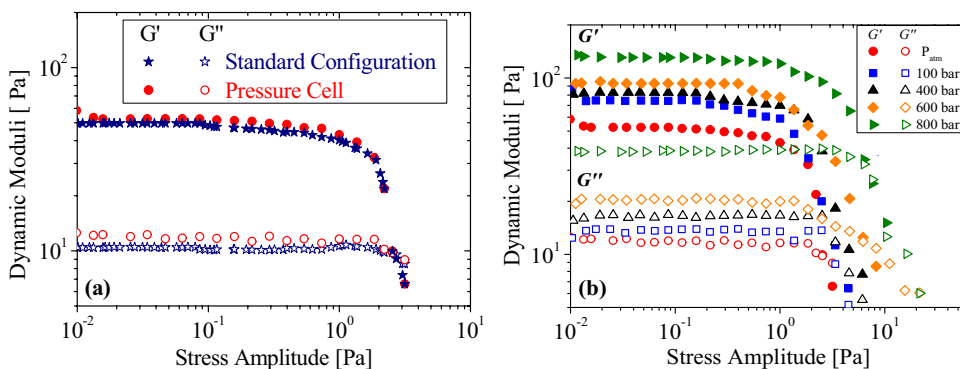


Fig. 3 Fitting the predicted values of the power-law model’s consistency coefficient as a function of pressure

Fig. 4 Oscillatory shear stress amplitude sweeps performed at 1 Hz and 25 °C. The dynamic moduli (G' and G'') as a function of the stress amplitudes at (a) atmospheric pressure (comparison between standard configuration and pressure cell), and (b) at different pressure



As shown in Fig. 4(a), the results obtained in both configurations at atmospheric pressure are similar. The main trends observed in the oscillatory shear stress amplitude sweep tests on standard configuration are also obtained by the tests on pressure cell configuration. As the order of magnitude of G' and G'' in all the regimes (SAOS, MAOS, and LAOS) are reliably determined by the pressure cell at atmospheric conditions, this configuration can be used to check the influence of higher pressure in this type of experimental protocol as shown in Fig. 4(b).

As can be seen, the higher the pressure experienced by the drilling fluid, the higher the dynamic moduli (G' and G''). Interestingly, the influence of the pressure is roughly the same in both moduli. In other words, $\delta \approx 13^\circ$ regardless of the imposed pressure. On the other hand, the crossover stress increased three times when the pressure increased from the atmospheric value to 800 bar as shown in Fig. 5. One can state that the higher the pressure, the higher the gel strength. In this figure, the standard deviations for three measurements is less than ± 0.35 Pa in all the applied pressures.

Based on the results presented in this section, one can conclude that the bentonite-free water-based drilling fluid presented yield stress and shear-thinning behavior, as reported in several studies in which xanthan gum solutions were examined (Norton et al. 1984; Choppe et al. 2010; N'gouamba et al. 2021). Many studies commonly argue that pressure is negligible for aqueous suspensions and that temperature is more predominant (Amani and Al-Jubouri 2012; Wang et al. 2012; William et al. 2014). This work displayed that pressure increases the material viscosity and the gel strength. In the next section, we study the influence of temperature on the rheological behavior of the BF-WBDF.

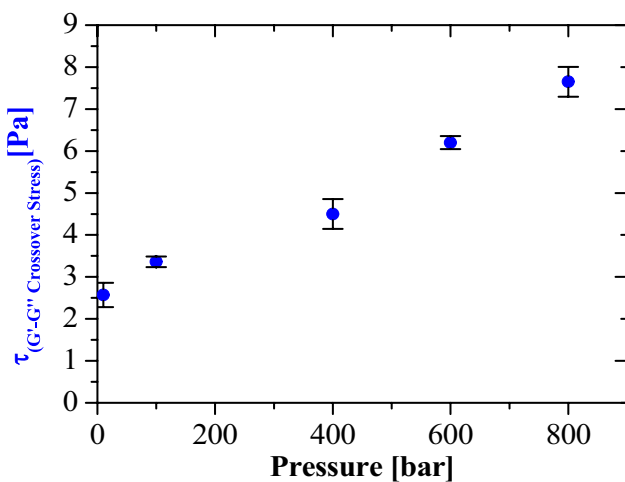


Fig. 5 Variation of the crossing stress ($\tau_{G' \text{ and } G''}$) as a function of pressure at 25 °C. The error bars denote the standard deviation of experiments performed in triplicate

Influence of the temperature

The effect of temperature is widely known for xanthan gum solutions (Higiro et al. 2007; Zhong et al. 2013; Reinoso et al. 2019). The use of xanthan gum in high-temperature drilling fluid has been investigated, and the fluid is susceptible to thermal degradation (Rochefort and Middleman 1987; Milas et al. 1990; Gulrez et al. 2012). Fluid thermostability is an essential key factor for engineering applications.

Therefore, it is fundamental to know the evolution of the effect of temperature in the free bentonite suspension of xanthan gum not only on the liquid-like but also on the solid-like regimes. Steady-state viscosity curves were carried out at 4, 10, 25, 40, 55, 70, 90, 100, and 125 °C in a wide range of shear rates from 50 to 400 s^{-1} and at a constant imposed pressure of 10 bar to avoid boiling at high temperatures. The time used in all tests for each step of shear rate was 1000 s. Figure 6 displays the apparent steady-state viscosity as a function of shear rate at different temperatures. The shear-thinning behavior was observed for all the imposed temperatures, and the higher the temperature, the lower the apparent viscosity.

It is worth noting that the influence of temperature is impacting values higher than 70 °C. It seems that the conformational changes of the xanthan gum from this temperature are more significant. Structural changes in xanthan gum can cause these effects; in other words, they can cause thermal degradation of the drilling fluid.

In this section, the power-law equation was also fitted to the apparent viscosity results. The fitted parameters for each temperature are presented in Table 3, as well as the fit parameters' uncertainty. Each of the fits was statistically

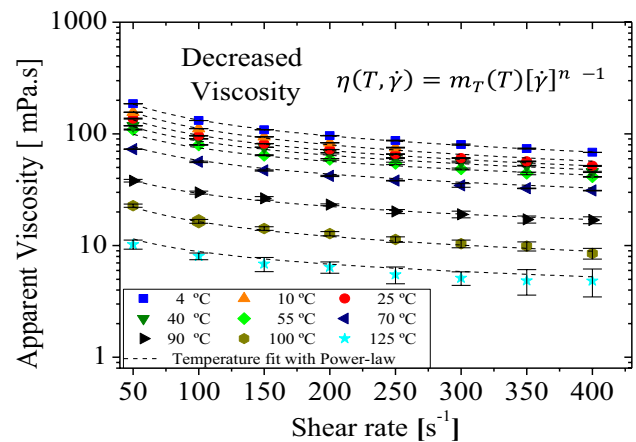


Fig. 6 Steady-state apparent viscosity curve at a different temperature from 4 to 125 °C were measurements at 10 bars on Anton Paar with Pressure Cell configuration, applying shear rate 400–50 s^{-1} . Experimental data were fitted by the modified power-law equation (dashed line). The error bars denote the standard deviation of experiments performed in triplicate

Table 3 Fitted parameters of the power-law equation at different temperatures. Consistency coefficient (m_T), flow behavior index (n_T), parameter uncertainties (δm_T and δn_T), mean squared error (MSE), and correlation coefficient (R^2)

Temperature [°C]	m_T [Pa.s ⁿ]	δm_T [Pa.s ⁿ]	n_T [-]	δn_T [-]	MSE	R^2
4	1188.2	28.82	0.53	0.005	1.34	0.999
10	1000.9	28.44	0.51	0.006	1.50	0.999
25	809.7	19.67	0.54	0.005	2.42	0.997
40	633.4	35.31	0.57	0.011	3.17	0.994
55	492.0	38.34	0.60	0.015	4.58	0.988
70	367.9	10.78	0.59	0.005	0.34	0.998
90	178.3	13.16	0.61	0.015	0.61	0.994
100	126.5	7.33	0.56	0.011	0.13	0.994
125	44.7	2.51	0.62	0.011	0.03	0.993

significant with p -values less than 0.001, indicating that the combined expanded uncertainty of the viscosity and temperature measurements is a 95% confidence level. The higher the temperature, the lower the consistency coefficient values (m_T) and the higher the flow behavior index (n_T). However, it is worth noting that the flow behavior index (n_T) is not much affected by the temperature. n_T varies from 0.53 to 0.62 when the temperature increases from 4 to 125 °C. Comparing the influence of the pressure (Table 2) and temperature (Table 3), temperature has a much more significant impact on the drilling fluid's rheological behavior.

Following the same line of thought of the previous section, the influence of temperature on the apparent viscosity is fitted using the WLF model proposed by Williams (1964). This model is based on molecular differences, which can predict the evolution of the rheological behavior for some fluids with polymer or biopolymer solutions when subjected to changes in temperature. As shown in Fig. 6, the temperature extraordinarily impacts the material's rheological behavior for values higher than 70 °C. Then, the behavior of the consistency coefficient values (m_T) was fitted in two different temperature ranges, as presented in Fig. 7. First, from 4 to 70 °C [dashed blue line] in which, the reference temperature was taken as 4 °C. For the second temperature range from 70 to 125 °C [dashed red line], it was necessary to find other fit parameters with a new reference temperature. For the second reference, temperature was chosen a transition temperature (T_m) of 70 °C, because the drilling fluid presented changes in structural configuration, therefore, changes in the rheological behavior of the material. Hence, a new fit was made with another reference temperature. One can understand this temperature as the conformational transition temperature (T_m), in which the polymeric chains of xanthan gum present an order-to-disorder structure transition. A calorimetric heating test was performed with this drilling fluid, and the result is presented in Appendix 1. One can observe an endothermic event around 70 °C during the heating of the sample. This event indicates that the polymeric chains are going through the conformation of the polymer chains

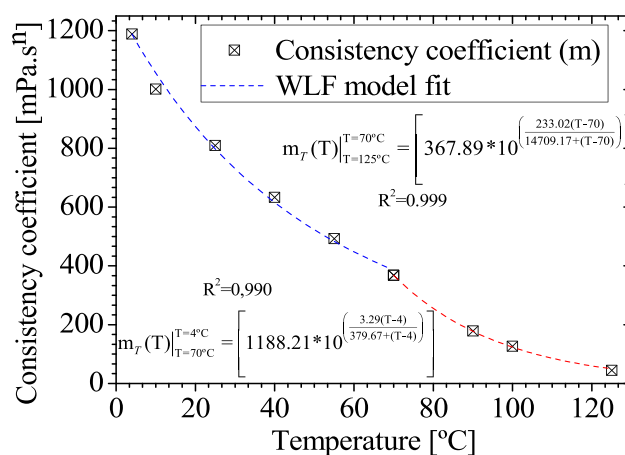


Fig. 7 Fitting of the predicted values of the power-law model's consistency coefficient as a function of temperature

process as discussed in the literature (Callet et al. 1989; Williams et al. 1991; Pelletier et al. 2001). Figure 7 shows the two models that describe each the temperature behavior. The fit parameters are indicated, which presented an R^2 of 0.990 and 0.999, respectively, indicating a good fit. In Appendix 3, a comparison between the predicted values and measured experimentally that ratifies the values of R^2 can be observed.

Analyzing the influence of the temperature on the rheological behavior of the drilling fluid in the solid-like regime, as performed in section “Influence of the pressures.” Stress amplitude sweep oscillatory tests were also conducted for different temperatures. The dynamic moduli (G' and G'') function of stress amplitude are presented in Fig. 8. The temperature strongly affects the characteristics of the material in the solid-like regime.

The higher the temperature, the lower the dynamic modulus in the SAOS region and the lower the crossover stress. For example, the storage modulus decreases by more than one order of magnitude, and the crossover stress decreases by almost two orders of magnitude (from ~ 3 to ~ 0.05 Pa) when the temperature increases from 4 to 125 °C (see

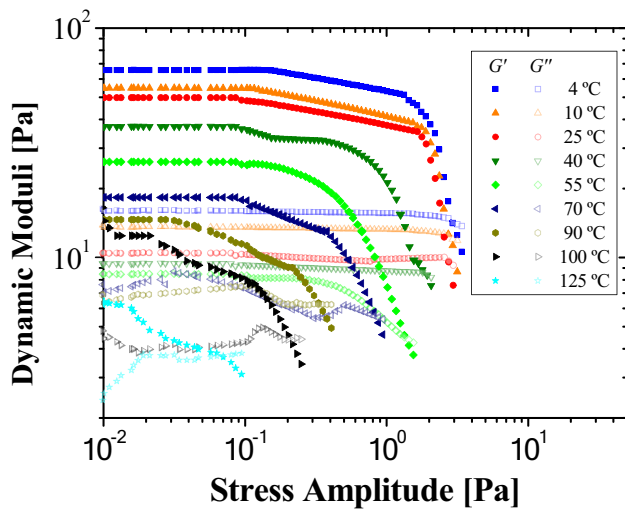


Fig. 8 Dynamic moduli as a function of stress amplitude for different temperatures. The oscillatory amplitude stress sweep tests were performed from 0.01 to 100 Pa at 1 Hz and constant imposed pressure of 10 bar

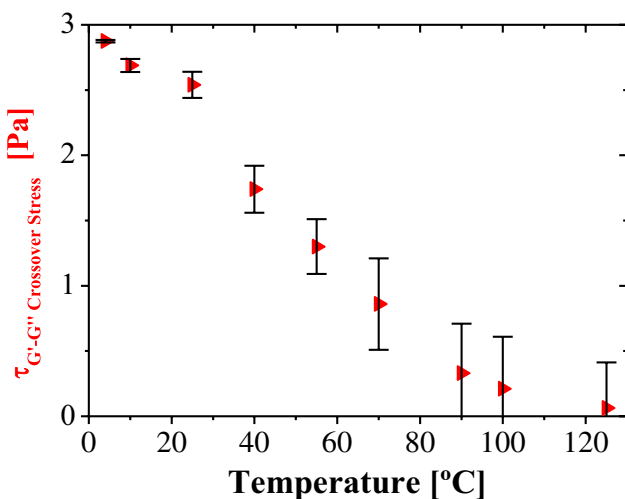


Fig. 9 Variation of the crossing stress ($\tau_{G' \text{ and } G''}$) as a function of temperature at atmospheric pressure. The error bars denote the standard deviation of experiments performed in triplicate

Fig. 9). In other words, the higher the temperature, the lower the drilling fluid gel strength.

The temperature that the material will experience is an important parameter to be analyzed before using the fluid in the drilling process. The knowledge of the temperature of the well is an essential parameter to predict the rheological behavior of the drilling fluid. Another question regarding the influence of the temperature is related to the possibility of irreversible effects of high temperatures on the drilling fluid behavior. In other words, does the material at ambient

temperature always have the same rheological behavior regardless of the thermal history? The following section will shed light on this discussion.

Effect of thermal aging

As discussed above, the rheological properties of the fluid are strongly dependent on temperature. As the xanthan gum presents a conformational transition temperature (T_m) from an order (helix) to disorder (coil) conformation, one could question if the effect of temperature on the rheological behavior is reversible or irreversible. In other words, whether the polymer chains tend to return to their helical form when the material is cooled again to lower temperatures. This question was analyzed using thermal aging tests. The drilling fluid was inserted in an aging cell at 6 bar and maintained for 16 h in a roller oven at four different temperatures ($T_{ag} = 55, 70, 100, \text{ and } 125 \text{ }^\circ\text{C}$). After the aging tests, the samples were stored for one day at 25 °C, as described in the “Materials and methods” section. Finally, the viscosity curves were measured in the rheometer.

Figure 10 presents the apparent viscosity in steady-state as a function of shear rate for three different test temperatures (a) 25 °C, (b) 55 °C, and (c) 70 °C. Each one of the curves represents different aging temperatures experienced by the samples. The four aged samples were compared with the unaged ones (blue circle). It is interesting to note that the $T_{ag} = 55 \text{ }^\circ\text{C}$ did not affect the material’s rheological behavior. In other words, the influence of the temperature up to this value is reversible even if the sample experiences this temperature level for 16 h. The apparent viscosity of the material is weakly affected by the thermal history when $T_{ag} = 70 \text{ }^\circ\text{C}$. These irreversible effects are more evident for $T_{ag} = 100 \text{ }^\circ\text{C}$ and significantly impact $T_{ag} = 125 \text{ }^\circ\text{C}$. The thermal degradations for $T_{ag} = 125 \text{ }^\circ\text{C}$ can irreversibly decrease the apparent viscosity in almost one order of magnitude. As previously reported (Mao et al. 2020) for $T_{ag} > T_m$, the suspension is destabilized, causing fluid degradation.

The results of the thermal aging tests were fitted to the power-law equation, as shown by the dashed lines in Fig. 10. Table 4 shows the consistency coefficient (m_{ag}) and the flow behavior index (n_{ag}) for the four aged samples and the unaged one at the three measured test temperatures.

It is worth noting in Table 4 that the thermal degradation affects the magnitude of the material’s apparent viscosity (as can be seen by the consistency coefficient) and affects the rheological behavior of the drilling fluid. In other words, the higher the aging temperature, for $T_{ag} > T_m$, the closer to 1 is the flow index (n_{ag}). The shear-thinning characteristics were not evident in these samples, and they present results closer to the Newtonian behavior.

It is important to emphasize that some authors investigated the addition of salts (Howard et al. 2015; Wu et al.

Fig. 10 Steady-state apparent viscosity as a function of shear rates at atmospheric pressure for three temperatures (a) 25 °C, (b) 55 °C, and (c) 70 °C. The curves represent the unaged and aged samples at $T_{ag} = 55, 70, 100,$ and 125 °C. The dashed line shows the power-law equation fitted to the results. The error bars denote the standard deviation of experiments performed in triplicate

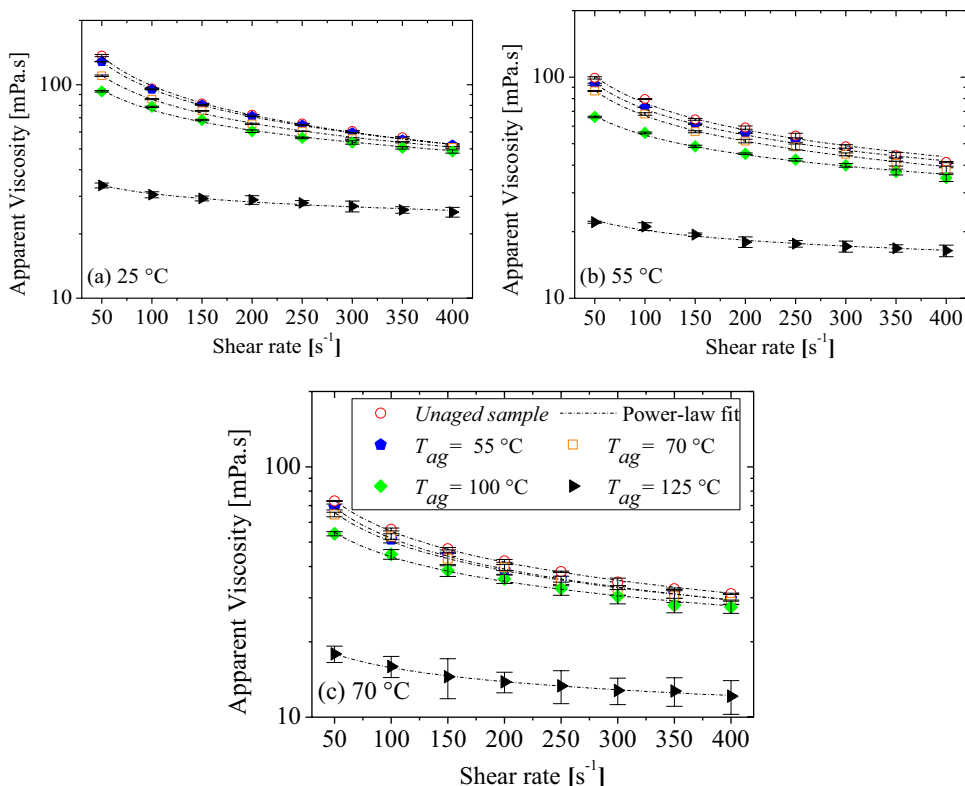


Table 4 Fitted parameters of the power-law equation at different aging and test temperatures. Consistency coefficient (m_{ag}), flow behavior index (n_{ag}), parameter uncertainties (δm_{ag} and δn_{ag}), mean squared error (MSE), and correlation coefficient (R^2)

Aging temperature T_{ag} [°C]	Test temperature 25 °C				Test temperature 55 °C				Test temperature 70 °C			
	m_{ag} [Pa.s ⁿ]	n_{ag}	R^2		m_{ag} [Pa.s ⁿ]	n_{ag}	R^2		m_{ag} [Pa.s ⁿ]	n_{ag}	R^2	
Unaged	809.7	0.54	0.997		492.0	0.60	0.988		367.9	0.59	0.998	
55	687.3	0.57	0.999		431.4	0.61	0.993		342.0	0.59	0.999	
70	474.9	0.63	0.997		386.9	0.62	0.995		298.8	0.61	0.998	
100	325.8	0.68	0.990		211.3	0.71	0.991		196.4	0.67	0.992	
125	56.1	0.87	0.974		40.6	0.85	0.960		36.9	0.82	0.995	
Aging temperature T_{ag} [°C]	Test temperature 25 °C				Test temperature 55 °C				Test temperature 70 °C			
	δm_{ag} [Pa.s ⁿ]	δn_{ag}	MSE		δm_{ag} [Pa.s ⁿ]	δn_{ag}	MSE		δm_{ag} [Pa.s ⁿ]	δn_{ag}	MSE	
Unaged	32.24	0.008	1.99		38.34	0.015	4.57		10.78	0.006	0.34	
55	7.19	0.002	0.12		24.60	0.011	2.16		7.17	0.004	0.15	
70	14.29	0.006	0.85		16.87	0.008	1.10		21.33	0.014	1.66	
100	17.72	0.010	2.21		10.38	0.009	0.93		9.76	0.009	0.61	
125	2.20	0.007	0.18		2.30	0.010	0.17		0.86	0.004	0.017	

2021) or nanoparticles (Vargas et al. 2020) to face the problems of low transition temperature and the degradation of the fluid due to thermal aging effects. William et al. (2014) performed an exciting analysis combining the effects of pressure and temperature on the rheological behavior of the drilling fluid. In this study, the pressures checked were limited to up 100 bar, and they concluded that the higher the temperature, the more impacting the influence of pressure. Based on this analysis, one interesting point for future works

is whether the imposition of pressure can increase the fluid’s conformational transition temperature (T_m).

Conclusions

The present experimental study investigated the influence of high pressure and high temperature on bentonite-free drilling fluids in which xanthan gum is used as the additive. The

rheometric experiments were developed with a pressure cell coupled to a rotational rheometer. Proposal procedures to fit equations to the results are presented. The main conclusions can be summarized below:

- (1) The higher the pressure imposed on the fluid, the higher the apparent viscosity and the gel strength of the drilling fluid.
- (2) The apparent viscosity curve can be well fitted using a power-law equation for any pressure imposed, and the flow behavior index (n) is roughly independent of the pressure. In other words, the pressure affects only the consistency coefficient (m), and this influence is higher in the low magnitude pressure range.
- (3) The influence of temperature is more impactful than that of pressure. The higher the temperature, the lower the material's apparent viscosity and gel strength.
- (4) The drilling fluid's rheological behavior is roughly independent of the thermal history of a specific temperature called conformational transition temperature (T_m). From this temperature on, the thermal history experienced by the fluid affects the material viscosity irreversibly.

It is important to emphasize that although the conformational transition temperature is well reported in the literature for fluids with xanthan gum, we proposed a methodology that can offer a model that predicts the material behavior at high pressures and up and down above the transition temperature. The findings presented in this work are valuable for drilling engineers. Based on these results, one can further understand the drilling fluid's behavior up to high pressure and temperatures. Finally, the analysis results using the best-fit approach to determine the apparent viscosity in the liquid regime and the dynamic moduli data on high pressures range in solid-regime remain a valuable addition to the toolbox of rheologists. The analysis of the polymer concentration, electrolytes, and addition of nanoparticles in the fluid, aiming to improve the thermally useful range of the bentonite-free drilling fluid, is a subject for future work.

Appendix 1. Calorimetric heating test

The transition temperature of the conformation of polymer chains process for bentonite-free water-based drilling fluid with xanthan gum was also investigated with the μ -DSC7 Evo microcalorimeter. The pre-test consisted of homogenizing the sample for 15 min in a Hamilton Beach HMD200 mixer at 1000 rpm, under standard temperature and pressure conditions. Then, with a single-channel micropipette, 0.5 mg of the drilling fluid was placed into the cell used for the samples, leaving the reference cell empty in the calorimeter. The

heating test was configured to control the temperature from 25 to 80 °C with a heating rate of 0.5 °C·min⁻¹.

Figure 11 shows a micro-DSC heating curve of bentonite-free water-based drilling fluid with xanthan gum. The curve displays an endothermic event starting at 67.08 °C and ending at 70.62 °C. The midpoint transition temperature T_m , is 69.24 °C. Therefore, according to Williams et al. (1991), one can conclude that this event represents the transition from an ordered to a disordered state of xanthan gum. In this specific case, this transition occurs at around 70 °C.

Appendix 2. Apparent viscosity as a function of time (pressure and temperature)

The variations of the apparent viscosity as a function of time for each shear rate plateau for the different temperatures were plotted in Fig. 12(a, b, c, d, e, f, g, h, i). Figure 13(a, b, c, d, e) presents the apparent viscosity as a function of time for different shear rates and imposed pressures.

Appendix 3. Comparison of predicted x measured values of apparent viscosity

The cross-plots were used to check the accuracy of established correlations. The output data for prediction were compared with the experimental results. Statistical parameters (i.e., the correlation coefficient (R^2) and the average absolute error (AAE)) were calculated. Figure 14 panels (a) and (b) show the experimental values and the fits developed for all temperatures and pressures applied in the experiments. It can be seen that the predicted values of the apparent viscosity coincide with the experimental results. In conclusion, the

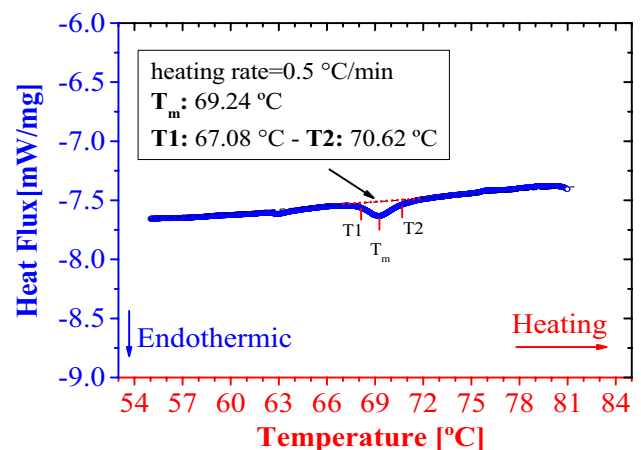


Fig. 11 Order–disorder transition of bentonite-free water-based drilling fluid with xanthan gum monitored by differential scanning microcalorimetry

Fig. 12 (a, b, c, d, e, f, g, h, i) Apparent viscosity as a function of time for successive plateaus of applied shear rates for different temperatures at 10 bar pressure

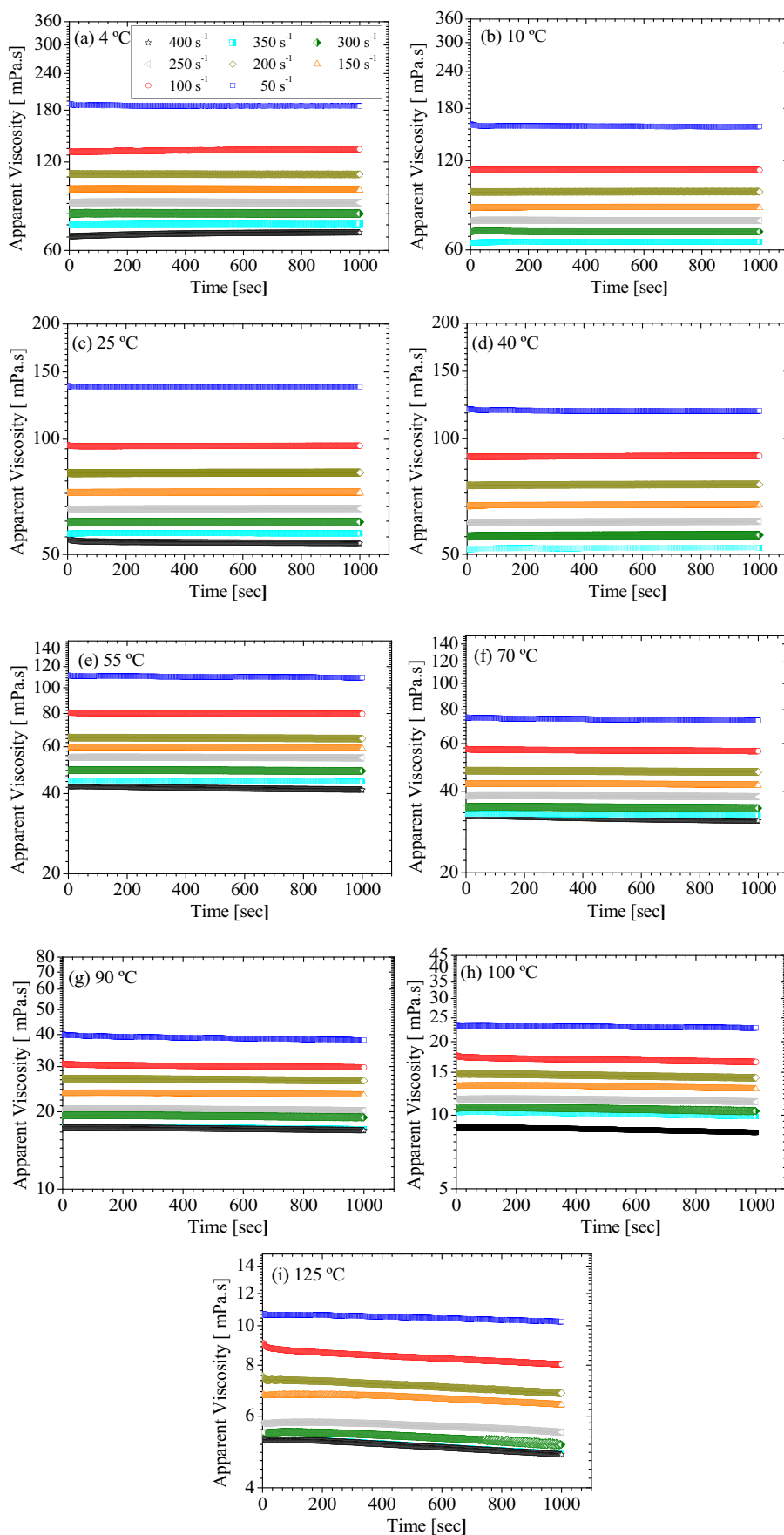


Fig. 13 (a, b, c, d, e) Apparent viscosity as a function of time at 25 °C for successive plateaus of applied shear rates for different pressure

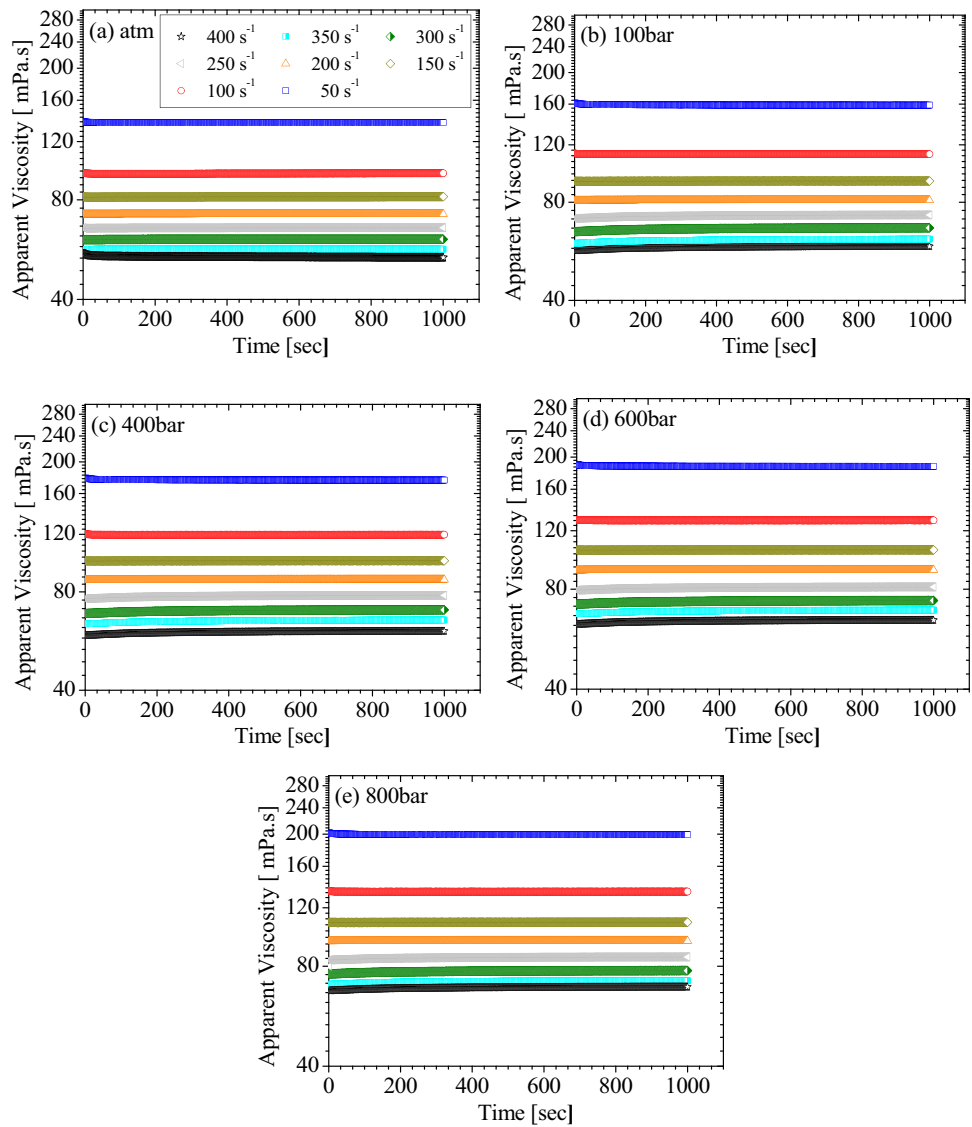
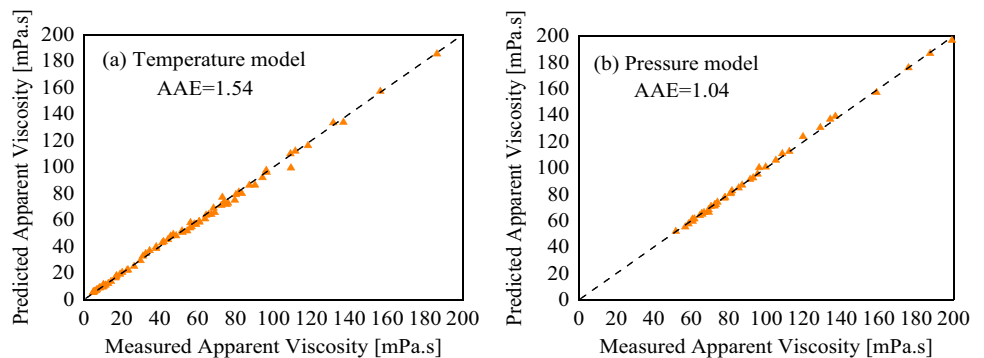


Fig. 14 Comparison of the measured and predicted values of the apparent viscosity: (a) temperature model and (b) pressure model



correlations predict the apparent viscosity with very high accuracy, for example, the pressure correlation has the highest R (99.99%) [Fig. 2b] and the temperature correlation was 99.90% [Fig. 6].

Nomenclature a [-]: The significance level; m [mPa.s ^{n}]: Consistency coefficient; n [-]: Flow behavior index; $\dot{\gamma}$ [s⁻¹]: Shear Rate; η [mPa.s]: Apparent Viscosity; A, B [mPa.s]: Empirical parameter the Barus Equation; α [-]: Viscosity-pressure coefficient; T, P [°C,

bar]: Temperature and Pressure; C_1 [–] and C_2 [°C]: Two empirical parameters of WLF model; G' [Pa]: Storage modulus; G'' [Pa]: Viscous modulus; δ [°]: Phase angle shift; T_m [°C]: Conformational transition temperature; δm [mPa.sⁿ]: Consistency coefficient uncertainties; δn [–]: Flow behavior index uncertainties; Subscript P (n_p , m_p): For pressure model; Subscript T (n_T , m_T): For temperature model; Subscript ag (n_{ag} , m_{ag} , T_{ag}): For aging model

Acknowledgements The authors also thank the Multilab LabReo CERNN/UTFPR for providing the rheometers used in the current work.

Funding The authors acknowledge the financial support of PETROBRAS S/A (TC 0050.0070318.11.9), CNPq (Process: 487091/2013–2), Coordenação de Aperfeiçoamento de Pessoal de Nível Superior – Brasil (CAPES) – Finance Code 001, FINEP, PRH-ANP/MCT (PRH-ANP/MCTI no. 10-C) and PFRH/PETROBRAS (6000.0067933.11.4 and 6000.0082166.13.4).

Declarations

Conflict of interest The authors declare no competing interests.

References

- Amani M, Al-Jubouri M (2012) The effect of high pressures and high temperatures on the properties of water based drilling fluids. *Energy Sci Technol* 4:27–33. <https://doi.org/10.5539/esr.v2n1p175>
- Andrade DEV, Fernandes RR, Santos TGM et al (2016) Curve-fitting equation for prediction of the start-up stress overshoot of an oil-based drilling fluid. *J Petrol Sci Eng* 146:902–908. <https://doi.org/10.1016/j.petrol.2016.07.037>
- Ansari S, Rashid MAI, Waghmare PR, Nobes DS (2020) Measurement of the flow behavior index of Newtonian and shear-thinning fluids via analysis of the flow velocity characteristics in a mini-channel. *SN Appl Sci* 2. <https://doi.org/10.1007/s42452-020-03561-w>
- API Recommended Practice 13B-1 (2017) Recommend practice for field testing water-based drilling fluids - 13B-1. API Publishing Services 2008:121
- Bagci S, Kok MV, Turksoy U (2000) Determination of formation damage in limestone reservoirs and its effect on production. *J Petrol Sci Eng* 28:1–12. [https://doi.org/10.1016/S0920-4105\(00\)00057-7](https://doi.org/10.1016/S0920-4105(00)00057-7)
- Callet F, Milas M, Rinaudo M (1989) On the role of thermal treatments on the properties of xanthan solutions. *Carbohydr Polym* 11:127–137. [https://doi.org/10.1016/0144-8617\(89\)90020-9](https://doi.org/10.1016/0144-8617(89)90020-9)
- Chaudemanche C, Henaut I, Argillier JF (2009) Combined effect of pressure and temperature on rheological properties of water-in-crude oil emulsions. *Appl Rheol* 19:1–8. <https://doi.org/10.3933/ApplRheol-19-62210>
- Choppe E, Puaud F, Nicolai T, Benyahia L (2010) Rheology of xanthan solutions as a function of temperature, concentration and ionic strength. *Carbohydr Polym* 82:1228–1235. <https://doi.org/10.1016/j.carbpol.2010.06.056>
- Donley GJ, Singh PK, Shetty A, Rogers SA (2020) Elucidating the G' overshoot in soft materials with a yield transition via a time-resolved experimental strain decomposition. *Proc Natl Acad Sci U S A* 117:21945–21952. <https://doi.org/10.1073/pnas.2003869117>
- Fann Instrument Company (2014) High temperature aging cell instruction manual. Fann Instrument Company, Houston. <https://www.fann.com>
- Fernandes RR, Andrade DEV, Franco AT, Negrão COR (2016) Correlation between the gel-liquid transition stress and the storage modulus of an oil-based drilling fluid. *J Nonnewton Fluid Mech* 231:6–10. <https://doi.org/10.1016/j.jnnfm.2016.02.003>
- Fernandes RR, Andrade DEV, Franco AT, Negrão COR (2017a) Influence of pre shearing on rheometric measurements of an oil-based drilling fluid. *Rheologica Acta* 56:743–752. <https://doi.org/10.1007/s00397-017-1027-y>
- Fernandes RR, DE Andrade V, Franco AT, Negrão COR (2017b) The yielding and the linear-to-nonlinear viscoelastic transition of an elastoviscoplastic material. *J Rheol* 61:893–903. <https://doi.org/10.1122/1.4991803>
- Fitzpatrick P, Meadows J, Ratcliffe I, Williams PA (2013) Control of the properties of xanthan/glucomannan mixed gels by varying xanthan fine structure. *Carbohydr Polym* 92:1018–1025. <https://doi.org/10.1016/j.carbpol.2012.10.049>
- Greenaway R, Parris M, Mueller F et al (2008) High-pressure, high-temperature technologies. *Oilfield Rev* 20:46–60
- Gulrez SKH, Al-Assaf S, Fang Y et al (2012) Revisiting the conformation of xanthan and the effect of industrially relevant treatments. *Carbohydr Polym* 90:1235–1243. <https://doi.org/10.1016/j.carbpol.2012.06.055>
- Hermoso J, Martínez-Boza F, Gallegos C (2014) Combined effect of pressure and temperature on the viscous behaviour of all-oil drilling fluids. *Oil Gas Sci Technol– Rev d'IFP Energies nouvelles* 69:1283–1296. <https://doi.org/10.2516/ogst/2014003>
- Higiro J, Herald TJ, Alavi S, Bean S (2007) Rheological study of xanthan and locust bean gum interaction in dilute solution: effect of salt. *Food Res Int* 40:435–447. <https://doi.org/10.1016/j.foodres.2006.02.002>
- Howard S, Kaminski L, Downs J (2015) Xanthan stability in formate brines - formulating non-damaging fluids for high temperature applications. SPE - European Formation Damage Conference, Proceedings, EFDC 2015-Janua:1388–1413. <https://doi.org/10.2118/174228-ms>
- Huang W, Xie B, Qiu Z, Jiang L (2016) Bentonite-free water-based drilling fluid with high-temperature tolerance for protecting peep reservoirs. *Chem Technol Fuels Oils* 51:652–662. <https://doi.org/10.1007/s10553-016-0655-8>
- Jang HY, Zhang K, Chon BH, Choi HJ (2015) Enhanced oil recovery performance and viscosity characteristics of polysaccharide xanthan gum solution. *J Ind Eng Chem* 21:741–745. <https://doi.org/10.1016/j.jiec.2014.04.005>
- Leusheva EL, Alikhanov NT (2021) Research of bare-free drilling fluids. *Недропользование* 21:123–130. <https://doi.org/10.15593/2712-8008/2021.3.4>
- Macosko CW (1994) *Rheology: principles, measurements and applications*. Wiley, New York
- Mao H, Yang Y, Zhang H et al (2020) A critical review of the possible effects of physical and chemical properties of subcritical water on the performance of water-based drilling fluids designed for ultra-high temperature and ultra-high pressure drilling applications. *J Petrol Sci Eng* 187:106795. <https://doi.org/10.1016/j.petrol.2019.106795>
- Mewis J, Wagner N (2012) *Colloidal suspension rheology*. New York
- Milas M, Rinaudo M, Knipper M, Schuppiser JL (1990) Flow and viscoelastic properties of xanthan gum solutions. *Macromolecules* 23:2506–2511. <https://doi.org/10.1021/ma00211a018>
- Morenov V, Leusheva E, Liu T (2021) Development of a weighted barite-free formate drilling mud for well construction under complicated conditions. *Polymers (Basel)* 13. <https://doi.org/10.3390/polym13244457>
- N'gouamba E, Essadik M, Goyon J et al (2021) Yielding and rheology of aqueous xanthan gum solutions. *Rheol Acta* 60:653–660. <https://doi.org/10.1007/s00397-021-01293-1>

- Navarrete RC, Himes RE, Seheult JM (2000) Applications of xanthan gum in fluid-loss control and related formation damage. SPE Permian Basin Oil and Gas Recovery Conference Proceedings. <https://doi.org/10.2118/59535-ms>
- Njobuenwu DO, Wobo CA (2007) Effect of drilled solids on drilling rate and performance. *J Petrol Sci Eng* 55:271–276. <https://doi.org/10.1016/j.petrol.2006.08.012>
- Norton IT, Goodall DM, Frangou SA et al (1984) Mechanism and dynamics of conformational ordering in xanthan polysaccharide. *J Mol Biol* 175:371–394. [https://doi.org/10.1016/0022-2836\(84\)90354-1](https://doi.org/10.1016/0022-2836(84)90354-1)
- Paar GmbH A (2015) Instruction Manual C-ETD 300/PR 1000. Anton Paar GmbH, Austria. <https://www.Anton-Paar.com>
- Patrick W, Hinrichs J, Kohlus R (2021) Macroscopic rheology of non-Brownian suspensions at high shear rate.pdf. 123–138
- Pelletier E, Viebke C, Meadows J, Williams PA (2001) A rheological study of the order-disorder conformational transition of xanthan gum. *Biopolymers* 59:339–346.
- Quainoo AK, Negash BM, Bavoh CB, Ganat TO, Tackie-Otoo BN (2020) A perspective on the potential application of bio-inhibitors for shale stabilization during drilling and hydraulic fracturing processes. *J Nat Gas Sci Eng* 79:103380. <https://doi.org/10.1016/j.jngse.2020.103380>
- Raheem AM, Vipulanandan C (2019) Salt contamination and temperature impacts on the rheological and electrical resistivity behaviors of water based drilling mud. *Energy Sources A: Recovery Util Environ Effects* 0:1–21. <https://doi.org/10.1080/15567036.2019.1587080>
- Reinoso D, Martín-Alfonso MJ, Luckham PF, Martínez-Boza FJ (2019) Rheological characterisation of xanthan gum in brine solutions at high temperature. *Carbohydr Polym* 203:103–109. <https://doi.org/10.1016/j.carbpol.2018.09.034>
- Rocheffort WE, Middleman S (1987) Rheology of xanthan gum: salt, temperature, and strain effects in oscillatory and steady shear experiments. *J Rheol* 31:337–369. <https://doi.org/10.1122/1.549953>
- Seright RS, Henrici BJ (1986) Xanthan stability at elevated temperatures. Society of Petroleum Engineers of AIME, (Paper) SPE 2:285–299
- Seymour KP, Macandrew R (1994) Design, drilling, and testing of a deviated HTHP exploration well in the North Sea. *SPE Drill Complet* 9:244–248. <https://doi.org/10.2118/26874-pa>
- Sofia GB, Djamel A (2016) A Rheological study of xanthan polymer for enhanced oil recovery. *J Macromol Sci Part B Phys* 55:793–809. <https://doi.org/10.1080/00222348.2016.1207544>
- Song K, Wu Q, Li MC et al (2016) Performance of low solid bentonite drilling fluids modified by cellulose nanoparticles. *J Nat Gas Sci Eng* 34:1403–1411. <https://doi.org/10.1016/j.jngse.2016.08.036>
- Sukhoboka O (2017) Drilling fluid rheology under high pressure high temperature conditions and its impact on the rate of penetration. Society of Petroleum Engineers - SPE Bergen One Day Seminar 2017. <https://doi.org/10.2118/185916-ms>
- Vargas J, Roldán LJ, Lopera SH et al (2020) Effect of silica nanoparticles on thermal stability in bentonite free water-based drilling fluids to improve its rheological and filtration properties after aging process. Offshore Technology Conference Brasil 2019, OTCB 2019. <https://doi.org/10.4043/29901-ms>
- Wang F, Tan X, Wang R et al (2012) High temperature and high pressure rheological properties of high-density water-based drilling fluids for deep wells. *Pet Sci* 9:354–362. <https://doi.org/10.1007/s12182-012-0219-4>
- Wei B, Romero-Zerón L, Rodrigue D (2014) Mechanical properties and flow behavior of polymers for enhanced oil recovery. *J Macromol Sci Part B Phys* 53:625–644. <https://doi.org/10.1080/00222348.2013.857546>
- Whitcomb PJ, Macosko CW (1978) Rheology of xanthan gum. *J Rheol* 22:493–505. <https://doi.org/10.1122/1.549485>
- William JKM, Ponmani S, Samuel R et al (2014) Effect of CuO and ZnO nanofluids in xanthan gum on thermal, electrical and high pressure rheology of water-based drilling fluids. *J Petrol Sci Eng* 117:15–27. <https://doi.org/10.1016/j.petrol.2014.03.005>
- Williams SA (1964) The effect of temperature on polyacrylate-and CMC-treated drilling muds. *J Appl Polym Sci* 8:1015–1022. <https://doi.org/10.1002/app.1964.070080237>
- Williams PA, Day DH, Langdon MJ et al (1991) Synergistic interaction of xanthan gum with glucomannans and galactomannans. *Top Catal* 4:489–493. [https://doi.org/10.1016/S0268-005X\(09\)80199-9](https://doi.org/10.1016/S0268-005X(09)80199-9)
- Wilson L, Wilson MJ, Green J, Patey I (2014) The influence of clay mineralogy on formation damage in North Sea reservoir sandstones: a review with illustrative examples. *Earth Sci Rev* 134:70–80. <https://doi.org/10.1016/j.earscirev.2014.03.005>
- Wu M, Shi Z, Ming Y et al (2021) Thermostable and rheological properties of natural and genetically engineered xanthan gums in different solutions at high temperature. *Int J Biol Macromol* 182:1208–1217. <https://doi.org/10.1016/j.ijbiomac.2021.05.008>
- Xia S, Zhang L, Davletshin A et al (2020) Application of polysaccharide biopolymer in petroleum recovery. *Polymers (basel)* 12:1–36. <https://doi.org/10.3390/POLYM12091860>
- Xie B, Liu X, Wang H, Zheng L (2016) Synthesis and application of sodium 2-acrylamido-2-methylpropane sulphonate/N-vinylcaprolactam/divinyl benzene as a high-performance viscosifier in water-based drilling fluid. *J Appl Polym Sci* 133:1–12. <https://doi.org/10.1002/app.44140>
- Zheng W, Wu X, Huang Y (2020) Impact of polymer addition, electrolyte, clay and antioxidant on rheological properties of polymer fluid at high temperature and high pressure. *J Petrol Explor Prod Technol* 10:663–671. <https://doi.org/10.1007/s13202-019-0732-8>
- Zhong C, Huang R, Ye L, Dai H (2006) Study on the morphology of the novel hydrophobically associative acrylamide-based terpolymer in aqueous solution by AFM measurements. *J Appl Polym Sci* 101:3996–4002. <https://doi.org/10.1002/app.22960>
- Zhong L, Oostrom M, Truex MJ et al (2013) Rheological behavior of xanthan gum solution related to shear thinning fluid delivery for subsurface remediation. *J Hazard Mater* 244–245:160–170. <https://doi.org/10.1016/j.jhazmat.2012.11.028>
- Zhou H, Deville JP, Davis CL (2015) Novel high density brine-based drill-in fluids significantly increased temperature limit for HP/HT applications. SPE/IADC Drilling Conference, Proceedings 2015-Janua: 1040–1052. <https://doi.org/10.2118/173075-ms>
- Zhu W, Zheng X (2021) Effective modified xanthan gum fluid loss agent for high-temperature water-based drilling fluid and the filtration control mechanism. *ACS Omega* 6:23788–23801. <https://doi.org/10.1021/acsomega.1c02617>

Publisher's note Springer Nature remains neutral with regard to jurisdictional claims in published maps and institutional affiliations.